研究成果の刊行に関する一覧表

雑　誌

発表者氏名	論文タイトル名	発表誌名	巻号	ページ	出版年
安永武史、福与恒雄、小西晃造、岡崎　賢、川辺善郎、洪　在成、小林毅一郎、家入里志、田上和夫、中島秀彰、橋爪　誠	先端CCD方式を用いたMRI対応内視鏡の開発	日本コンピュータ外科学会誌	7(3)	327-328	2005
T.Yasunaga, T.Fukuyo, K.Tanoue, K.Konishi, K.Okazaki, J.Hong, S.Ieiri, H.Nakashima, M.Hashizume	MRI-compatible Endoscope to use distally-mounted CCD	The proceeding of the 2006 SAGES Annual Meeting		273-274	2006
T.Yasunaga, K.Konishi, S.Yamaguchi, K.Okazaki, J.Hong, S/Ieiri, H.Nakashima, K.Tanoue, T.Fukuyo, M.Hashizume	MR-compatible laparoscope with a distally mounted CCD for MR image-guided surgery	International Journal of Computer Assisted Radiology and Surgery	2(1)	11-18	2007
Hashizume M	MRI-guided laparoscopic and robotic surgery for malignancies	International Journal of Clinical Oncology	12(2)	94-98	2007

Ⅲ　研究成果の刊行物・別冊

Int J CARS (2007) 2:11–18
DOI 10.1007/s11548-007-0076-6

ORIGINAL ARTICLE

MR-compatible laparoscope with a distally mounted CCD for MR image-guided surgery

Takefumi Yasunaga · Kozo Konishi · Shohei Yamaguchi · Ken Okazaki · Jae-sung Hong · Satoshi Ieiri · Hideaki Nakashima · Kazuo Tanoue · Tsuneo Fukuyo · Makoto Hashizume

Received: 25 December 2006 / Accepted: 6 March 2007 / Published online: 12 May 2007

Abstract
Objects We have developed a new MR-compatible laparoscope that incorporates a distally mounted charge-coupled device (CCD). The MR-compatibility and feasibility of laparoscopy using the new laparoscope were evaluated during MR image-guided laparoscopic radiofrequency ablation therapy (RFA).
Materials and methods MR compatibility of the laparoscope was investigated in terms of MR image artifact caused by electromagnetic interference (EMI) and susceptibility. MR images were obtained using spin echo and gradient echo pulse sequences with a 0.3 T open MRI unit. We performed an in vivo experiment with MR image-guided laparoscopic RFA on three pigs; near real-time MR images and 3-D navigation were possible using intraoperative MR images. Agarose gel was injected into the pigs' livers as puncture targets; the diameter of each target was approximately 20 mm.
Results Artifacts resulting from EMI were not found in phantom experiments. MR image-guided laparoscopic RFA was successfully performed in all procedures. Both the laparoscopic vision and near real-time MR images were clear. No artifact was detected on the MR images and the surgeon was able to confirm the true position of the probe and target during treatment using the near real-time MR images.
Conclusion Laparoscopic surgery is feasible under intraoperative MR image-guidance using a newly developed MR-compatible laparoscope with a distally mounted CCD.

Keywords MR-compatible laparoscope · MR-compatibility · Susceptibility artifact · Electromagnetic interference · MR image-guided laparoscopic radiofrequency ablation

T. Yasunaga · K. Konishi · S. Yamaguchi · K. Okazaki · J.-s. Hong · H. Nakashima · M. Hashizume (✉)
Department of Advanced Medical Initiatives, Faculty of Medical Sciences, Kyushu University, 3-1-1, Maidashi, Higashi-ku, Fukuoka city, Fukuoka 812-8582, Japan
e-mail: mhashi@dem.med.kyushu-u.ac.jp

T. Yasunaga
e-mail: t-yasu@surg2.med.kyushu-u.ac.jp

K. Konishi
e-mail: Konizou@surg2.med.kyushu-u.ac.jp

S. Yamaguchi
e-mail: shohei@surg2.med.kyushu-u.ac.jp

K. Okazaki
e-mail: Okazaki@med.kyushu-u.ac.jp

J.-s. Hong
e-mail: hong@dem.med.kyushu-u.ac.jp

H. Nakashima
e-mail: hnaka@dem.med.kyushu-u.ac.jp

S. Ieiri · K. Tanoue · M. Hashizume
Department of Advanced Medicine and Innovative Technology, Kyushu University Hospital, 3-1-1, Maidashi, Higashi-ku, Fukuoka city, Fukuoka 812-8582, Japan
e-mail: satoshi@pedsurg.med.kyushu-u.ac.jp

K. Tanoue
e-mail: tanoue_k@dem.med.kyushu-u.ac.jp

T. Fukuyo
Shinko Optical Co. Ltd., 2-12-2, Hongo, Bunkyo-ku, Tokyo 113-0033, Japan
e-mail: shinko-koki@par.odn.ne.jp

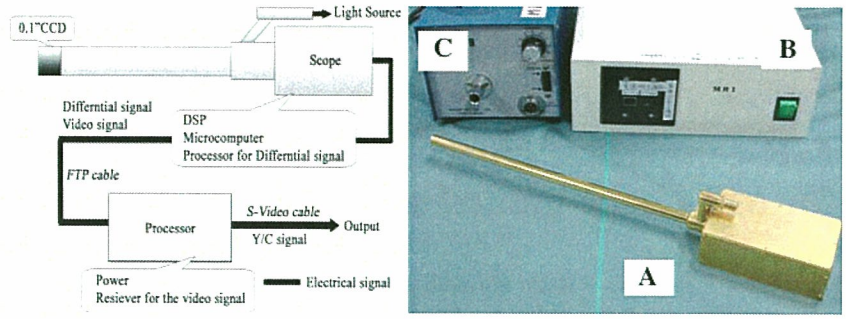

Fig. 1 Design of the MR-compatible laparoscope with a distally mounted CCD. A diagram of the design is shown on the *left*, and a prototype is shown on the *right*. *A*, *B*, and *C* indicate the MR-compatible laparoscope with a distally mounted CCD, signal processor and the light source, respectively

Introduction

Intraoperative magnetic resonance (MR) imaging is a useful system for evaluating the effects of treatment and as a surgical targeting tool for brain tumors [1]. Laparoscopic surgery has developed dramatically during the past decade [2], with recent studies reporting the use of intraoperative MR imaging in laparoscopic surgery [3–6] based on a conventional laparoscope with an additional charge-coupled device (CCD) located on the proximal side of the laparoscope. These laparoscopes are made of MR-compatible materials and are not attracted by the magnetic field; however, artifact was caused by electromagnetic interference (EMI) when the proximally mounted CCD approached the center of the magnet. We have developed a new MR-compatible laparoscope with a distally mounted CCD that does not cause EMI artifact when the CCD approaches the center of the magnet.

We used phantoms to evaluate MR-compatibility and evaluated the feasibility of the system by performing MR image-guided laparoscopic radiofrequency ablation on three pigs.

Materials and methods

Design of MR-compatible laparoscope with a distally mounted CCD

A conventional laparoscope consists of a relay substrate comprising an object lens and an eyepiece, a CCD, and a processor that includes a digital signal processor (DSP) and microcomputer. Image artifact on MR images is caused by EMI from electrical noise emitted from equipment such as laparoscopes, resulting in the degradation of MR image quality. EMI is generated by the electric signals that pass through the long cable connecting the CCD and processor; this phenomenon is known as the antenna effect [7]. We adopted differential signaling to decrease EMI because shielding of the scope and cables alone was insufficient. A 0.1-in. CCD (ICX256FKW, SONY, Tokyo, Japan) was placed at the distal side of the scope, and an electrical circuit that included a microcomputer, processor, and DSP was placed at the proximal side of the scope (Fig. 1). The DSP had a clock frequency lower than 12.6 MHz, which is the nuclear magnetic resonance frequency of 0.3 T MRI. The scope was double-wrapped with cupronickel to ensure the safety of the patient in the event of a short circuit. Cupronickel was used because it produced less image artifact than brass in preliminary studies (Fig. 2).

MRI apparatus and RF receiver coil

The MR image was obtained using a 0.3 T open MRI unit (AIRIS-II, Hitachi, Tokyo, Japan) and a prototype thin body coil (W: 430 mm; H: 300 mm; D: 50 mm). The body coil was designed for intraoperative use.

MR-compatible display system

An MR-compatible display system was set up that enabled the laparoscopic image to be viewed in the MRI room (Fig. 3). The system consisted of a liquid crystal display (LCD)

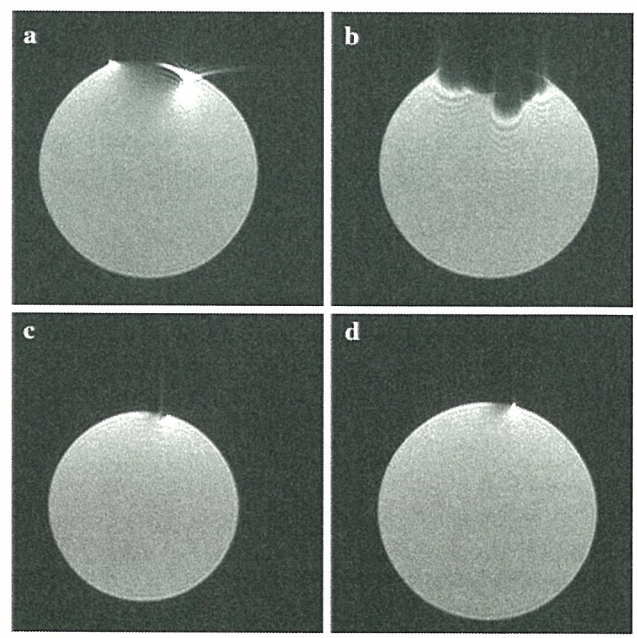

Fig. 2 Image artifact caused by brass and cupronickel. The images at the top of the figure demonstrate artifact caused by brass imaged using spin echo (**a**) and gradient echo (**b**). Those on the bottom demonstrate artifact caused by cupronickel imaged using spin echo (**c**) and gradient echo (**d**)

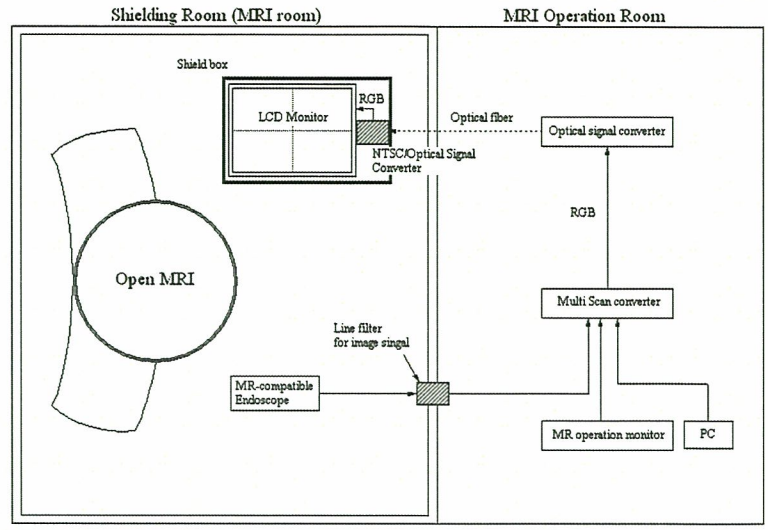

Fig. 3 MR-compatible display system

monitor, electromagnetic monitor shield, optional NTSC-optical signal converter, flexible optical fiber, and the multi-scan converter. The multi-scan converter has four image channels: an MR image, navigation image, and laparoscopic view can be displayed. The scan converter was placed outside the MRI room to prevent degradation of MR image quality; the video signal of the laparoscope was transferred from the MRI room through a line noise filter (Fig. 3).

Assessment of imaging artifact related to electromagnetic interference

We measured signal-to-noise ratio (SNR) to evaluate the influence on MR image quality caused by EMI; this was performed while changing the position of the laparoscope within the magnet. SNR was measured three times at each position (distance between the image plane and the tip of the laparoscope: −5, 0, 5, and 10 cm), perpendicular to the image plane (Fig. 4). These measurements were performed in the two phase-encoding directions (A-P and R-L) of the gradient magnetic field to determine the scan parameters that produced the least artifact. The images were obtained using spin echo (TR/TE, 500/40; thickness, 5.0 mm; FOV, 260 mm, scanning time, 1.0 min) and gradient echo sequences (TR/TE, 30/11.5; thickness, 10.0 mm; FOV, 300 mm; scanning time, 3.8 s.), called near real-time MR imaging. A commercially available phantom (Hitachi Medical Corp., Tokyo, Japan) that included 18 mmol/l $NiCl_2$ and 0.5 w/v % NaCl was placed in the gantry during image acquisition. Spin echo was used to evaluate the severity of artifacts by multiplying a given noise, while gradient echo was used for evaluation in conditions that resembled the clinical setting. Near-real-time MR imaging was used for navigation during MR image-guided laparoscopic radiofrequency ablation therapy (RFA). A near real-time image was obtained with the laparoscope located within the magnet. SNR was calculated according to the following formula: $SNR = SI_{ROI}/SD_{BACK}$, where SI_{ROI} is the average value of pixel intensity in the region of interest (ROI) on the phantom and SD_{BACK} is the average value of the standard deviations measured in four background regions of interest. The size of the ROI was uniform in all calculations. We calculated the decrease in MR image quality (DQ) caused by EMI using the following formula: $DQ(\%) = (SNR_{OBJ} - SNR_{CTR})/SNR_{CTR} \times 100$, where SNR_{OBJ} was measured while the laparoscope was in use, and SNR_{CTR} was measured with the laparoscope not in use and removed from the magnetic field.

Assessment of imaging artifact related to susceptibility of the MR-compatible laparoscope

We assessed the influence of the MR-compatible laparoscope on the MR image, distortion, and signal loss using a grid phantom (Fig. 5). The grid phantom consisted of orthogonal

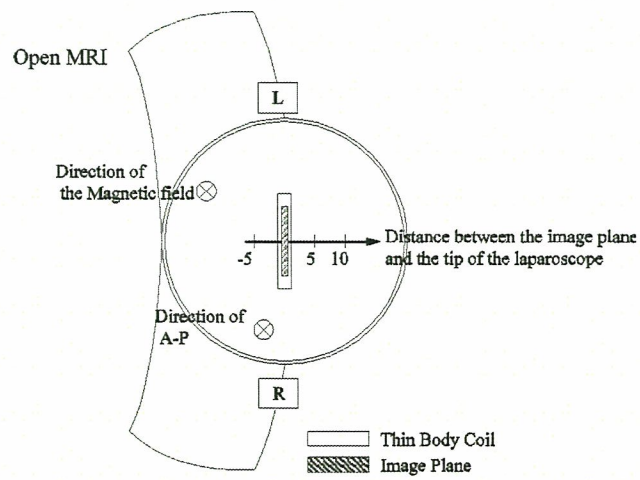

Fig. 4 Position of the laparoscope in the EMI experiment

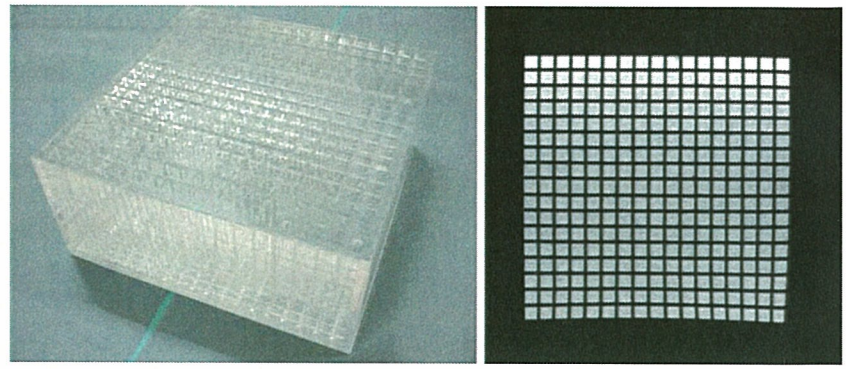

Fig. 5 Grid phantom. The *left-hand* figure is a view of the grid phantom (H: 178 mm, W: 178 mm, D: 80 mm) that was filled with H_2O. The *right-hand* figure is the MR image obtained using spin echo at the upper surface of the grid phantom

grooves separated by acrylic plates at 10 mm intervals. The phantom was filled with H_2O before being placed at the center of the magnet; a single transverse MR image was obtained 10 mm from the surface of the phantom using gradient echo, which was the sequence employed for near real-time MR imaging (TR/TE, 30/11.5; thickness, 10.0 mm; FOV, 300 mm; scanning time, 3.8 s.). These MR images were obtained with the laparoscope placed at various angles (22.5°, 45°, 90°, 135°, and 157.5°.) and distances (1, 2, 3, 4, and 5 cm) from the MR image plane at the center of the gantry, and with two different phase encoding directions (A-P and R-L) of the gradient magnetic field (Fig. 6). The influence on the MR image was evaluated by counting the number of grooves that demonstrated distortion or signal loss. MR images were obtained five times at each position.

Preclinical evaluation of the MR-compatible laparoscope in vivo

The protocol was approved by the Animal Care and Use Committee, Kyushu University. The laboratory animals for this study were handled and cared for according to national and institutional guidelines. MR image-guided laparoscopic radiofrequency ablation was performed in 3female pigs with a mean body weight of 25 kg (range, 23–28 kg). The animals were given no food 24 h prior to the interventions.

General anesthesia was induced with intravenous injection of 0.05 mg/kg atropine sulfate 0.5 mg (Tanabe, Osaka, Japan), 15 mg/kg ketamine hydrochloride (Ketalar 50, Sankyo Co. Ltd., Tokyo, Japan), and 0.5 mg/kg mesylate mafoprazine (MAFROPANE, Dainippon Sumitomo Pharma Co. Ltd., Osaka, Japan). The animals underwent intubation and mechanical ventilation using a mixture of oxygen, nitrous oxide, isoflurane (FORANE, Abbott Japan Co. Ltd., Tokyo, Japan), and room air, with MR-compatible anesthesia machinery (Aestiva/5^{TM} MRI, GE Medical Systems, UK). The vital signs of animals were monitored with MRI vital signs monitoring (Pulse ox meter 4500, Konica Minolta Holdings Inc., Japan) at all times. At the conclusion of the study, the animals were euthanized with an intravenous injection of concentrated pentobarbital solution (NEMBUTAL, Dainippon Sumitomo Pharma Co. Ltd., Osaka, Japan) and KCl solution (Conclyte, Otsuka Pharmaceutical Co. Ltd., Tokyo, Japan).

We used a target based on agarose gel to mimic a tumor. The gel consisted of 2.5% agarose (H14 TAKARA, Takara Bio Inc., Otsu, Japan) and 0.5% Gd-DTPA-BMA (Omniscan, Daiichi Pharmaceutical Co. Ltd, Tokyo, Japan). We decided

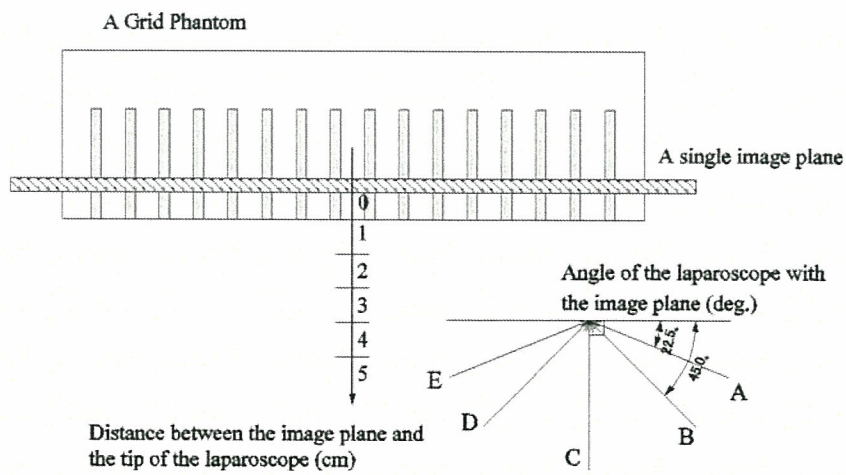

Fig. 6 Position of the laparoscope in the susceptibility experiment

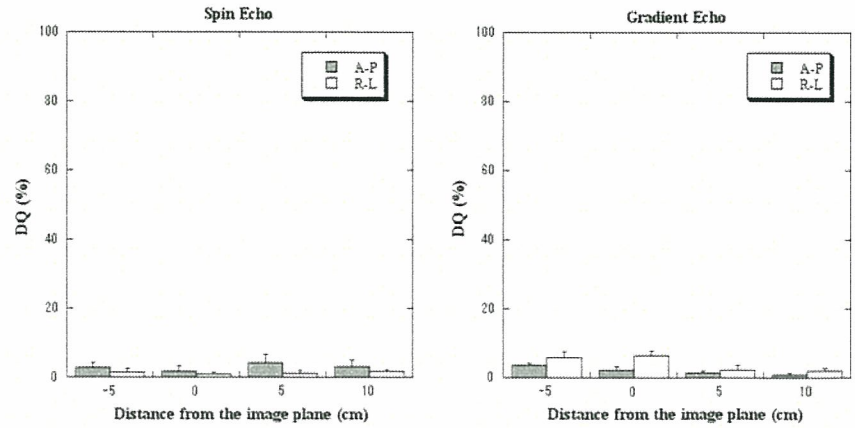

Fig. 7 Susceptibility artifact caused by the MR-compatible laparoscope at each position

the proper concentration of Gd-DTPA-BMA enhanced in both near real-time MR imaging and in 3-D MR imaging for 3-D navigation. The agarose gel was heated to 80°C; 4.0 ml of gel was injected into the liver of each pig using a 14 G needle. The injection site was cooled locally with ice for a short time to promote solidification of the gel. Each target was verified to have a diameter of approximately 2 cm on the MR image. We used an MR-compatible RFA probe made from titanium with a length of 15 cm that incorporated a 17-gauge electrode (Cool-tip, Valleylab, Tycohealthcare, USA.). An optical marker was attached to the probe, and the 3-D position of the probe was measured using an optical tracking system (Polaris, Northern Digital Industry Inc., Canada). We used gradient echo to obtain near real-time MR images that verified needle position on the basis of these data. The surgeon used the volume data from the MR images (3DT1, GE; FOV, 260 mm; TR/TE, 20/8.0; slice thickness, 5.0 mm; interval, 50; Flip Angle, 40; NSA, 3; matrix, 224 × 128, scan time, 3.0 min) to determine the 3-D position of the tool in relation to the target. The probe can be controlled and its real-time 3-D position and orientation confirmed because the probe indicator is projected onto the MR volume data. All equipment, including the laparoscope, was sterilized and tested for ferromagnetism using a simple hand-held magnet before being brought into the MRI room. The punctures for the mimic tumors were performed under laparoscopic vision using near real-time MR imaging and 3-D navigation.

Statistical analysis

All data were expressed as average values ± standard error of measurement (SEM). The influence on the MR image of distortion or signal loss was compared for each position of the laparoscope using the t-test ($P > 0.05$, Bonferroni correction).

Results

Assessment of imaging artifact related to electromagnetic interference

We did not find artifact related to EMI at any position in either the spin echo or gradient echo images, even when the CCD located at the distal side of the laparoscope was placed at the center of the magnetic field. The MR image quality did not decrease at any position because the change in DQ was less than ±10% (Fig. 7). There was no significant difference between the DQ of the two phase encoding directions in all positions ($P < 0.05$).

Assessment of imaging artifact related to susceptibility of the MR-compatible laparoscope

A susceptibility artifact caused by the laparoscope was recognized as distortion and signal loss on the MR images (Fig. 8). Signal loss was evident in both the A-P and R-L phase encoding directions; distortion was prominent in the A-P direction but subtle in the R-L direction. Both distortion and signal loss disappeared at 4 cm in position A, C, D, and E; the artifacts disappeared at 3 cm in position B. In all positions, the artifact in the R-L direction was less pronounced than that in the A-P direction. When the laparoscope was located 2–3 cm from the image plane, the artifact in the R-L direction was particularly insignificant compared to that in the A-P direction for all angles ($P > 0.05$).

Preclinical evaluation of the MR-compatible laparoscope in vivo

We performed MR image-guided laparoscopic radiofrequency ablation successfully on three pigs using the newly developed laparoscope. All of the surgical tools including the laparoscope were tested for ferromagnetic properties using a

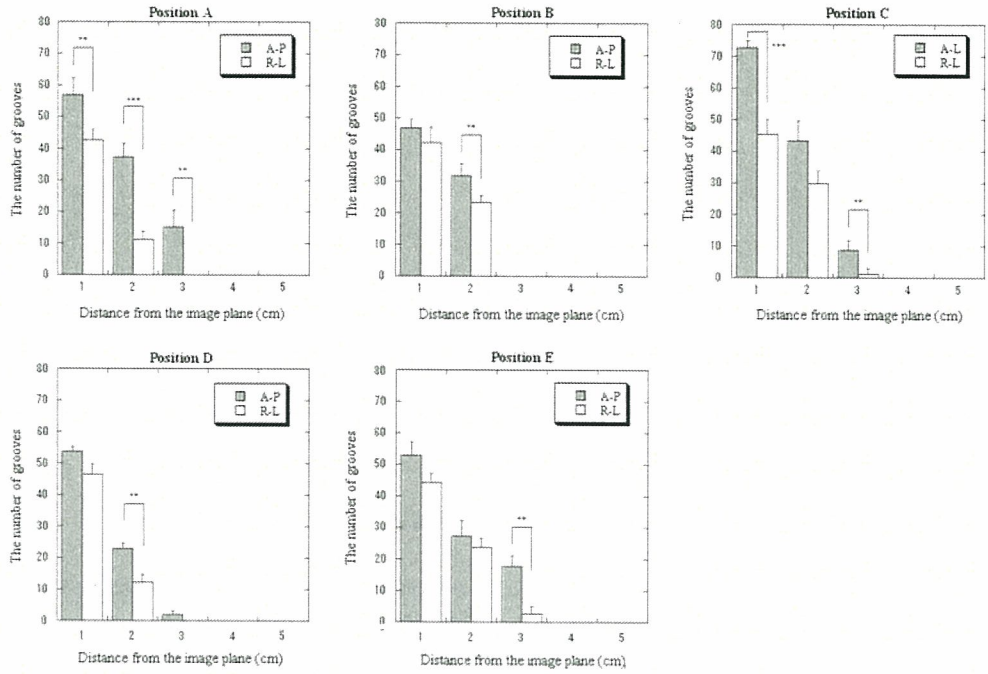

Fig. 8 Artifact caused by electromagnetic interference. The results for spin echo are displayed on the *left*. The results for gradient echo are displayed on the *right*. The *negative numbers* indicate the distance that the distal end of the scope passes through the image plane. * $P < 0.05$ ** $P < 0.01$ *** $P < 0.001$

simple handheld magnet. The laparoscope was not attracted to the magnetic field and was easily controlled in the magnetic field by the scopist. The surgeon successfully punctured the mimic tumor using multi-image information. No artifact related to EMI from the laparoscope, was found in the near-real-time MR images; however, EMI was detected from other electronic equipment including the MR-compatible anesthesia machinery and MRI vital signs monitoring. These artifacts disappeared when the equipment was located approximately 1 m from the five-gauss line. The signal loss and distortion detected when the laparoscope approached within 3 cm of the MR image plane in the phantom experiment were not found in the near real-time MR images. Laparoscopic vision was clear during the scanning (Fig. 9), and the surgeon was able to locate the position of the probe and target for 3-D navigation at all times. This system enabled confirmation of the true position of the probe and target during treatment via near real-time MR imaging. The laparoscope was used to confirm that there was no bleeding from the puncture site.

Discussion

We have successfully developed a new MR-compatible laparoscope.

The ASTM defines the following conditions of MR-compatibility for a foreign device: it is MR safe and has been demonstrated to neither significantly affect the quality of the diagnostic information nor have its operations affected by the MR device [8]. We consider that an MR-compatible laparoscope must satisfy the following requirements:

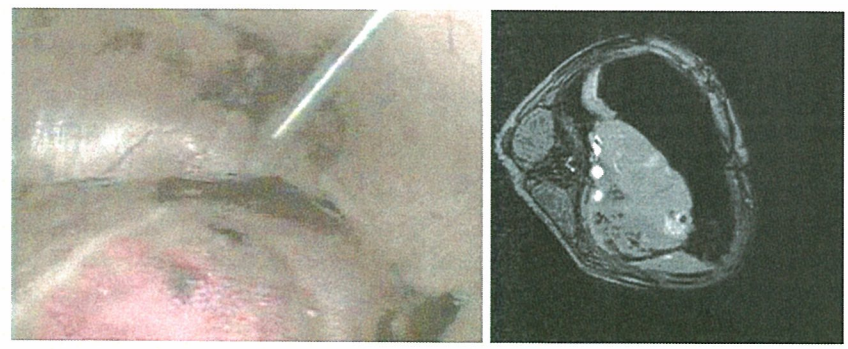

Fig. 9 Laparoscopic view during MR image-guided laparoscopic radiofrequency ablation surgery in vivo (image captured from movie) and near real-time MR image. Laparoscopic vision is shown on *the left*, and near real-time MR image is shown on *the right*

the laparoscope works normally in the MR environment, the scopist can control the laparoscope as in conventional laparoscopic surgery even in the MR environment, and its use in MR image-guided laparoscopic surgery does not affect MR image quality. It is necessary to evaluate image quality in terms of imaging artifact related to EMI, which is generated by electric signals passing through the long cable that connects the CCD and the processor, in addition to artifact related to the susceptibility of the laparoscope.

Artifact resulting from EMI was not detected, even when the distally mounted CCD approached the image plane. Other MR-compatible laparoscopes have the CCD at the proximal side of the scope, and consist of rigid relay lenses, an object lens, and an eyepiece [3–6]. It is comparatively easy to shield a laparoscope of this design for EMI because the camera head and optical coupler can be eliminated from the MRI gantry; however, we adopted differential signaling because it is impossible to eliminate the CCD from the MRI gantry using a laparoscope with a distally mounted CCD. It is very important that an artifact resulting from EMI is not found even if the distally mounted CCD were to be placed at the center of the magnetic field: this indicates that an issue in the development of flexible-tip versions of the MR-compatible laparoscope has been solved. The scopist cannot freely control the laparoscope in laparoscopic surgery under intraoperative MRI because of the confines of the narrow space. A flexible MR-compatible laparoscope is required to enable the surgeon to obtain a wide range of laparoscopic vision using MRI, as in conventional laparoscopy. Our concept of newly developed MR-compatible laparoscope with a distally mounted CCD will assist in the development of a flexible MR-compatible laparoscope and will enable laparoscopic surgery to be performed more easily under intraoperative MRI. Furthermore, one report has found that a laparoscope with a distally mounted CCD was superior in terms of consistently clear image quality because there is no honeycomb effect from the fiber bundle when compared to a conventional laparoscope, in which the CCD is placed on the proximal side of the scope [9]. The diameter of our scope can become smaller because the CCD is able to perform well even with less light. Therefore, our new MR-compatible laparoscope may be superior to existing MR-compatible laparoscopes with proximally mounted CCD.

The distally mounted CCD caused susceptibility artifact; however, according to the results of the susceptibility experiment, artifact does not occur when the CCD is more than 4 cm from the image plane. A previous report evaluated tissue interaction in a simulation using a turkey as a phantom [10]; however, distortion without signal loss cannot be assessed with such a phantom. Distortion would not be detected even if the MR image of a turkey phantom were distorted because the signal intensity is identical in all parts. We consider that distortions that are not visible on the turkey phantom could cause misplacement of image information in actual MR imaging. We were able to evaluate this invisible distortion using a grid phantom. In the present study, susceptibility artifact had little affect when the phase encoding direction was set in the R-L direction.

We confirmed that the laparoscope was MR-safe by testing with a handheld magnet. Although this test is very simple, it is useful as a preliminary test to evaluate the attraction of an unknown instrument to the MR magnet [11]. In the present study, the scopist could easily control the laparoscope in the magnet and it had no affect on near real-time MR imaging in the in vivo experiment. We consider that the laparoscope came no closer than 4 cm to the MR image plane because the scopist controlled the laparoscope in order to confirm placement of the RFA probe, other forceps, and the puncture site of the liver. MR-compatibility for medical devices is described in detail by Woods [12], who stated that a device is MR-compatible unless the amount and location of artifact affects the region of interest to the clinician, and that a complete absence of artifact is not always desirable. It was confirmed that our laparoscope produced image artifact in phantom experiment, but near real-time MR imaging was not affected by the use of our scope during MR image-guided laparoscopic RFA. Therefore, it is feasible to apply this MR-compatible laparoscope prototype to MR image-guided radiofrequency ablation therapy. Importantly, MR-compatibility depends on the MR conditions [8]. The laparoscope should be retested before use in different MR conditions, for example in a higher magnetic field.

All punctures were successfully performed by RFA probe using our laparoscope with near real-time MR imaging and 3-D navigation. RFA is usually performed percutaneously under ultrasound (US) guidance; however, laparoscopic or thoracoscopic RFA has advantages over the percutaneous approach because the subphrenic area or free surface of the liver can be punctured safely and easily [13,14]. US is the standard guidance modality for RFA, but it has a relatively low sensitivity in detecting hepatocellular carcinoma (HCC) with liver cirrhosis [15,16]. It is reported that the computed tomography (CT) guidance has limitations such as radiation dose [17,18]. MR image-guided laparoscopic RFA using our MR-compatible laparoscope solves all of the above issues. MRI guidance provides the surgeon with image verification of the probe at all times, as with US guidance, and the image plane can be obtained in any orientation. MR fluoroscopy delivers no radiation dose. In our in vivo experiment, the surgeon was able to easily guide the probe close to the mimic tumor on the first attempt using 3-D navigation; the true positions of the target and probe could then be confirmed, and the puncture could be completed via near real-time MR imaging. We consider that MR image-guided laparoscopic RFA is safer and more effective and precise than percutaneous RFA performed under US or CT.

Previous studies report that MR image-guided laparoscopic surgery is feasible for other procedures in addition to local ablation treatment for tumors. Lauro et al. [5] performed intraoperative MR-cholangiography using fast spin echo during laparoscopic cholecystectomy. Intraoperative MRI will ameliorate safety issues in laparoscopic cholecystectomy because MR-cholangiography is much less invasive for patients compared to conventional cholangiography [19]. Recent research reports MR imaging for lymph nodes [20, 21]. Our MR-compatible laparoscope, near real-time MR imaging, and 3-D navigation is likely to be used to assist the surgeon dissecting lymph nodes under intraoperative MRI.

In conclusion, we have developed a new MR-compatible laparoscope that incorporates a distally mounted CCD. We performed MR image-guided laparoscopic RFA more safely, effectively, and precisely than percutaneous RFA performed under US or CT. This MR-compatible laparoscope with distally mounted CCD is useful in laparoscopic surgery under intraoperative MR image guidance; use of this laparoscope will improve the safety of conventional laparoscopic surgery.

Acknowledgements We are grateful to Media Technology Corporation in Japan for measurement for the EMI of the laparoscope. This project was supported by the Ministry of Health, Labor, and Welfare, Japan (H16-trans-006).

References

1. Muragaki Y, Maruyama T, Iseki H, Hori T, Takakura K (2004) Intraoperative MRI and updated navigation. Nippon Rinsho 62(4): 697–706
2. Hashizume M, Takenaka K, Sugimachi K, Hepatectomy (1996) In: McFadyen BV Jr., Ponsky JL (eds) Operative laparoscopy and thoracoscopy, Lippincott-Raven, Phiadelphia, pp 387–408
3. Melzer A, Schmidt A, Kipfmüller K, Grönemeyer D, Seibel R (1997) MR-compatible instruments for interventional MR. In: Fuflin RB (ed) Interventional MRI. Mosby, St. Louis, pp 55–69
4. Morikawa S, Inubushi T, Kurumi Y, Naka S, Sato K, Tani T, Haque HA, Tokuda J, Hata N (2003) New assistive devices for MR-guided microwave thermocoagulation of liver tumors. Acad Radiol 10(2): 180–88
5. Lauro A, Gould SW, Cirocchi R, Giustozzi G, Darzi A (2004) Laparoscopic and general surgery guided by open interventional magnetic resonance. Minerva chirurgica 59(5): 507–16
6. Kataoka H, Chinzei K, Washio T, Iseki H, Hori T, Fukuyo T (2000) Development of MR Compatible Endoscope. proc JSCAS 2000: 173–174
7. Hayes DL, Holmes DR, Gray JE (1987) Effect of 1.5 tesla nuclear magnetic resonance imaging scanner on implanted permanent pacemakers. J Am Coll Cardiol 10(4): 782–786
8. Designation:F2119–01 (2007) Standard test method for evaluation of mr image artifacts from passive implants, ASTM International, West conshohocken
9. Olympus News Release (2004) Olympus EndoEYE^{TM}. Surgical Videoscope Receives "Innovation of the Year Award" From Society of Laparoendoscopic Surgeons
10. Frank G. Shellock, Vincent J. Shellock (1998) Spelzer Titanium Aneurysm Clips: Compatibility at MR Imaging. Radiology. 206(3):838–841
11. Gould SWT, Gedroyc W, Darzi A (1999) Laparoscopic surgery in a 0.5-t interventional magnetic resonance unit. Surg Endosc 13: 604–610
12. Woods TO (2003) MRI Safety and compatibility of implants and medical devices, stainless steels for medical and surgical applications, ASTM STP 1438. In: Winters GL, Nutt MJ (eds) ASTM International, West Conshohocken
13. Santambrogio R, Bianchi P, Palmisano A, Donadon M, Moroni E, Montorsi M (2003) Radiofrequency of hepatocellular carcinoma in patients with liver cirrhosis: a critical appraisal of the laparoscopic approach. J Exp Clin Cancer Res 22(4): 251–255
14. Santambrogio R, Podda M, Zuin M, Bertolini E, Bruno S, Comalba GP, Cosa M, Montorsi M (2003) Safety and efficacy of laparoscopic radiofrequency of Hepatocellular carcinoma in patients with liver cirrhosis. Surg Endosc 17: 1826–32
15. Dodd 3rd GD, Mller WJ, Baron RL, Skolnick ML, Campbell WL (1992) Detection of malignant tumors in end-stage cirrhotic livers: efficacy of sonography as a screening technique. AJR Am J Roentgenol 159: 727–733
16. Kim CK, Lim JH, Lee WJ (2001) Detection of Hepatocellular carcinomas and dysplastic nodules in cirrhotic liver: accuracy of ultrasonography in transplant patients. J Ultrasound Med 20: 99–104
17. Kim YJ, Raman SS, Yu NC, Lu DSK (2005) MR-guided percutaneous ethanol injection for hepatocellular carcinoma in a 0.2 T open MR system. J Magn Reson Imaging 22: 566–571
18. Martin RCG (2005) Intraoperative magnetic resonance imaging ablation of hepatic tumors. Am J Surg 189: 388–394
19. Nickkholgh A, Soltaniyekta S, Kalbasi H (2006) Routine versus selective intraoperative cholangiography during laparoscopic cholecystectomy: a survey of 2,130 patients undergoing laparoscopic cholecystectomy. Surg Endosc 20(6): 868–74
20. Mack MG, Balzer JO, Straub R, Eichler K, Vogl TJ (2002) Superparamagnetic iron oxide-enhanced MR imaging of head and neck lymph nodes. Radiology 222: 239–244
21. Kato M, Saji S, Kanematsu M, Fukada D, Miya K, Umemoto T, Kunieda K, Sugiyama Y, Takao H, Kawaguchi Y, Takagi Y, Kondo H, Hoshi H (1999) Detection of Lymph-node metastases in patients with gastric carcinoma: comparison of three MR imaging pulse sequences. Abdom Imaging 25: 25–29